Theoretical and Experimental Study of High-Peak-Power High-Brightness Quasi-CW Fiber Laser

Li Wang, Hanwei Zhang, Peng Wang, Baolai Yang, Xiaolin Wang, Yu Ning, and Xiaojun Xu

***Abstract*—The main factors limiting the power scaling of high-peak-power high-brightness quasi-continuous wave (QCW) fiber laser oscillator and a possible solution are analyzed in this paper. The impacts of fiber length and grating parameters on the output power are studied by rate equations. Under the optimized parameters, a high-brightness QCW fiber laser oscillator with a peak power of 7.3 kW is presented experimentally by using a 24 meter long spindle-shaped Yb-doped fiber with a constant core cladding ratio, and that is the best performance of peak power and brightness in near-single-mode QCW fiber lasers at present to the best of our knowledge. The corresponding pulse energy is 0.57 J and the beam quality M^2 factor is about 1.43 under the condition of repetition frequency of 1 kHz and pulse width of 100 μs. The details are analyzed, and also the limiting factors of further power scaling, strategies of suppressing nonlinear effects and the principle of optical device parameter optimization.**

***Index Terms*—Fiber lasers, ytterbium, high-power fiber lasers (HPFL), quasi-continuous wave (QCW), near-single-mode.**

I. Introduction

AS THE remarkable advantages of high power density, high efficiency, good heat dissipation, and compactness, high energy fiber lasers have been widely used in many fields [1], [2]. While in amounts of the applications, several kilowatts peak power and several joules pulse energy are simultaneously required, where the traditional continuous wave (CW) lasers or pulse lasers cannot be fully competent. Therefore, the QCW fiber lasers with a comparatively low repetition (0.5–50 kHz) and high peak power (1.5–20 kW) came to being, and have been proved to hold a better performance than the CW fiber lasers or the pulse fiber lasers with ∼mJ level pulse energy in laser surface melting [3], laser additive manufacturing [4], high speed cutting [5], laser cleaning [6], direct fabrication of single-crystal-like structures [7], and so on. Although the same peak and average power can be obtained by modulating a kW ytterbium doped fiber laser, the price and volume advantage of QCW fiber laser are significant [5].

Several commercial QCW fiber laser products can be easily accessed for the moment. However, the peak power of near-single-mode (M^2<1.5) QCW products does not exceed 2 kW up to now (e.g., YLM 200/2000, produced by IPG photonics inc., USA, max peak power 1.5 kW, $M^2 = 1.05$), and those with peak power higher than 2.5 kW are generally operated in multi-modes, with a BPP more than 1.5 mm·mrad (e.g., YLR 450/4500, IPG photonics inc., max peak power 4 kW, BPP ≥2 mm·mrad). One obvious reason is that, in order to obtain higher power and suppress the nonlinear effects, larger core diameter gain fibers should be used, while the number of high-order modes supported by the fibers increases at the same time, making the near-single-mode operation scarcely possible.

In fact, the laser intensity is not only decided by the power, but also the beam quality, that is the brightness. The relative brightness can be adopted to characterize the comprehensive performance of lasers, using the formula [2]

$$B_r = P_{peak}/\left(\lambda M^2\right)^2/100$$

where the wavelength λ is in microns. Here, the relative brightness of a fiber laser with a peak power of 10 kW and a beam quality factor of $M^2 = 10$ at 1.0 μm is defined 1.0 as the reference. According to this definition, the relative brightnesses of the two commercial QCW fiber laser products mentioned above are 11.9 and 1.14, respectively.

In previous studies, a 15 meters long double cladding fiber of core/cladding diameter 30/400 μm was adopted to achieve a nearly 10 kW peak power QCW fiber laser [8], but the beam quality M^2 factor exceeds 2.3, corresponding to a relative brightness of 16.0. In order to control the beam quality and increase the relative brightness, we focus on a new type of spindle-shaped gain fiber, as shown in Fig. 1, whose core and cladding diameters vary with longitude as the same ratio, which has been theoretically and experimentally verified to have many advantages, such as excellent capacity of suppressing nonlinear effects, and maintaining good beam quality [9]–[11]. Specifically, *Yang, etc.* in [12] took a 19 meter long 21/400 μm active fiber to achieve a 3.05 kW fiber laser oscillator in 2018,

Manuscript received April 13, 2022; revised May 3, 2022; accepted May 6, 2022. Date of publication May 10, 2022; date of current version May 20, 2022. This work was supported in part by the Training Program for Excellent Young Innovations of Changsha under Grants kq2106004 and kq2106008 and in part by the National Natural Science Foundation of China under Grants 61905282 and 62005315. *(Corresponding authors: Hanwei Zhang; Xiaolin Wang.)*

Li Wang is with the College of Advanced Interdisciplinary Studies, National University of Defense Technology, Changsha, Hunan 410073, China (e-mail: 13545486054@163.com).

Hanwei Zhang, Peng Wang, Baolai Yang, Xiaolin Wang, Yu Ning, and Xiaojun Xu are with the College of Advanced Interdisciplinary Studies, National University of Defense Technology, Changsha, Hunan 410073, China, and also with the State Key Laboratory of Pulsed Power Laser Technology and the Hunan Provincial Key Laboratory of High Energy Laser Technology, Changsha, Hunan 410073, China (e-mail: zhanghanwei100@163.com; 1169723259@qq.com; yangbaolai1989@163.com; chinawxllin@163.com; ningyu_0205@126.com).

Digital Object Identifier 10.1109/JPHOT.2022.3173992

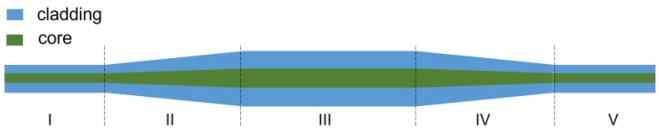

Fig. 1. The diagrammatic drawing of a spindle-shaped YDF.

corresponding to a beam quality M^2 factor ∼1.3, and stimulated Raman scattering (SRS) intensity ∼29 dB lower than that of the signal. Two years later, in 2020, *Zeng, etc.* in [9] achieved the same power with a much longer (31m) spindle-shaped gain fiber, whose both ends' core/cladding diameters were 20/400 μm. The M^2 factor of the output laser in that experiment was also ∼1.3, but the SRS intensity was much lower, about 31 dB lower than that of the signal, experimentally demonstrating the superiority of the spindle-shaped gain fibers in those scopes where needed to suppress SRS while maintaining a good beam quality.

After simulation and optimization, a 7.3 kW peak power near-single-mode ($M^2 = 1.43$) QCW fiber laser oscillator with an excellent SRS intensity ∼24 dB lower than that of the signal is demonstrated in this manuscript by utilizing a spindle-shaped gain fiber, corresponding to an exciting relative brightness of 31.4, much higher than ever before.

II. Theory Simulation and Cavity Optimization

The output power of a QCW fiber laser can be calculated from the rate equations (REs). The main simulation equations are

$$N_0 = N_1 + N_2 \tag{1}$$

$$\frac{\partial N_2}{\partial t} = \frac{1}{hc}\int \frac{\Gamma_p}{A_p}\lambda_p \left[\sigma_p^a N_1 - \sigma_p^e N_2\right]\left[P_p^+ + P_p^-\right]d\lambda + \frac{1}{hc}\int \frac{\Gamma_s}{A_s}\lambda_s \left[\sigma_s^a N_1 - \sigma_s^e N_2\right]\left[P_s^+ + P_s^-\right]d\lambda - \frac{N_2}{\tau} \tag{2}$$

$$\pm\frac{\partial P_p^\pm}{\partial z} + \frac{1}{v_p}\frac{\partial P_p^\pm}{\partial t} = \Gamma_p\left[\sigma_p^e N_2 - \sigma_p^a N_1\right]P_p^\pm - \alpha_m^p P_p^\pm \tag{3}$$

$$\pm\frac{\partial P_s^\pm}{\partial z} + \frac{1}{v_s}\frac{\partial P_s^\pm}{\partial t} = \Gamma_s\left[\sigma_s^e N_2 - \sigma_s^a N_1\right]P_s^\pm - \alpha_n^s P_s^\pm + \Gamma_s P_s^\pm \int \frac{1}{A_s} g_R(\Delta\omega)\left[P_s^+ + P_s^-\right]d\lambda + f_{SE} \tag{4}$$

where

Γ	power overlap factor;
A	effective area of the optical field;
λ	laser wavelength;
σ^a	absorption cross section of the doped ion;
σ^e	emission cross section of the doped ion;
α	attenuation coefficient;
h	Planck constant;
c	light velocity in vacuum;
τ	life time of the excited state;
P	power of laser;
v	group velocity of laser;
g_R	Raman gain;
f_{SE}	spontaneous emission.

TABLE I
Values of Major Simulation Parameters

Parameter	Value	Parameter	Value
λ_p	976nm or 960-980nm	λ_s	1070nm or 980-1150nm
Γ_p	0.0056	Γ_s	0.9
N_0	4.28×10^{25}/m^3	τ	0.84ms
α_p	0.003/m	α_s	0.005/m
σ_p^a	1.77×10^{-24}m^2	σ_s^a	4.5×10^{-27}m^2
σ_p^e	1.71×10^{-24}m^2	σ_s^e	3.63×10^{-25}m^2
R_1	0.999	R_2	0.108

N_1 and N_2 respectively stand for the numbers of doped ions per unit volume in the ground state, and in the excited state. The superscript $+/-$ denote the co-/counter-propagating cases, and the subscript s, p denote the signal and pump, respectively. The integral symbol means to calculate the entire pump or signal wavelengths considered in the simulation. The REs above can be solved by finite-difference method [13]. Note, that the length step size and time step size should satisfy the relationship of $dz = vdt$ to model the physical propagation of the optical field [14].

The values of the major simulation parameters are shown in Table I. The core/cladding diameters of the active fiber are set to be 30/400 μm. The reflective spectral shapes of the two FBGs are assumed to be Gaussian, and the 3 dB bandwidths are respectively 4.09 nm (R1) and 1.98 nm (R2), consisted with the values of experiment. To balance the simulation accuracy and efficiency, the time step size and time window are set to be $3.3\times10^{-10}s$ and $1\times10^{-3}s$.

A. The Impact of Active Fiber Length Under Different Pump Wavelengths

The authors in [8] verified the feasibility of QCW fiber laser by a simplified RE simulation just considered one single wavelength of pump and signal. However, the actual pump spectrum contains far more than one frequency component, and this may be one of the main reasons for the relatively low conversion compared to the CW operation in a QCW fiber laser. Specifically, the experimental pump spectrum envelope is shown in Fig. 2(a). The integral energy nearby 976 nm is just a half of all, and mounts of pump energy distributes in the area of 960–974 nm where the normalized absorption ratio is significantly lower than that of 976 nm. In this manuscript, the actual spectrum envelop of the pump is taken into consideration. The simulation results of output power and optical efficiency under different active fiber lengths are shown in Fig. 2(b). It can be seen that the efficiency declines with the increase of the fiber length when assuming that the pump spectrum just contains one single wavelength of 976 nm (blue line). The decline is mainly caused by the laser attenuation in the fiber core, therefore it maintains a good linearity. When taking multiple pump wavelengths into consideration, the optical efficiency gradually increases until the maximum conversion efficiency is reached (red line). That is mainly because the absorption ratio in the area of 960–974 nm

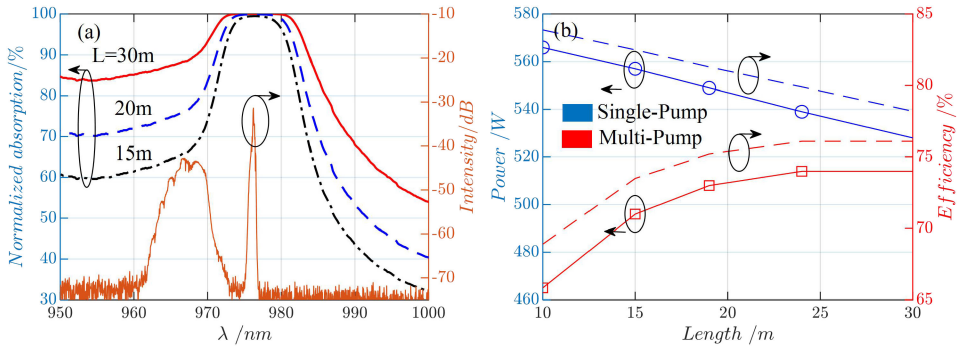

Fig. 2. (a) The spectrum of counter-pump at 667 W (brown), and the normalized absorption ratio after 24 m spindle-shaped YDF at each wavelength. (b) Output powers and optical efficiencies under different fiber lengths.

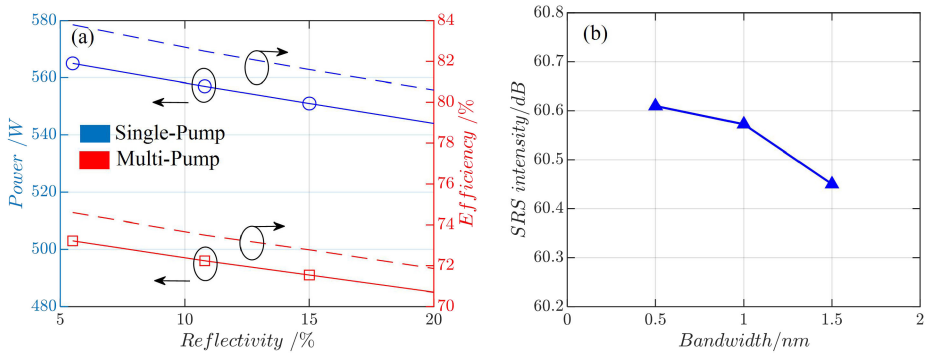

Fig. 3. (a) The output powers and efficiencies of QCW under different reflectivities of OC-FBG; (b) The SRS intensities under different FWHMs of OC-FBG.

would gradually improve as the active fiber length increases, as shown in Fig. 2(a). For that case in the simulation, a length of 20–25 m is appropriate to get a higher output power.

B. The Impact of Different OC Grating Parameters

Average output powers and optical efficiencies under different reflectivities of output coupling fiber Bragg grating (OC-FBG) are simulated, as shown in Fig. 3(a). It can be seen that with the decrease of the reflectivity, the output power and optical efficiency increase linearly, and the variation trends are the same in the two cases. When considering the SRS effects, the variation of SRS intensity with the FBG's bandwidth is calculated as shown in Fig. 3(b). It can be seen that the SRS intensity decreases gradually with the bandwidth, which is consistent with the reported experimental and simulation results [13], [15]. It should be noted that, we picked the power just after the OC-FBG as the basis for comparison, which reflects the influence of the grating parameters on the Raman intensity generated inside the cavity, and excludes the influence of the subsequent delivery fiber. No matter how long the GDF outside the cavity is, it has no effect on the Raman intensity generated inside the cavity. The greater the Raman intensity of the laser after the OC-FBG, the greater the Raman intensity after passing through the same GDF, and their changing trends with the grating parameters are consistent.

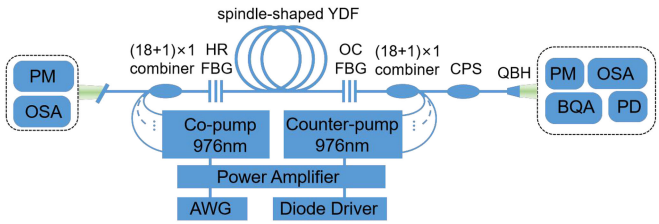

Fig. 4. Schematic of the experimental setup (PD: photodetector, PM: power meter, OSA: optical spectrum analyzer, FBG: fiber Bragg grating, HR: high reflection, YDF: ytterbium-doped fiber, OC: output coupling, CPS: cladding power stripper, QBH: quartz block head, BQA: beam quality analyzer, AWG: arbitrary waveform generator).

According to the simulation results above, a 24 meters long spindle-shaped gain fiber, and the OC-FBG with a reflectivity and bandwidth about 5.5% and 1.01 nm was picked in the following experiments.

III. Experimental Setup

A typical structure of bidirectional-pumped fiber laser oscillator was adopted for the following experiments is shown in Fig. 4, except that the active fiber was a long spindle-shaped gain fiber with a constant core/cladding diameter ratio, whose lengths of Sections I to V were 2m-6m-8m-6m-2m, respectively, and its core/cladding diameters varied from 25/400 μm to

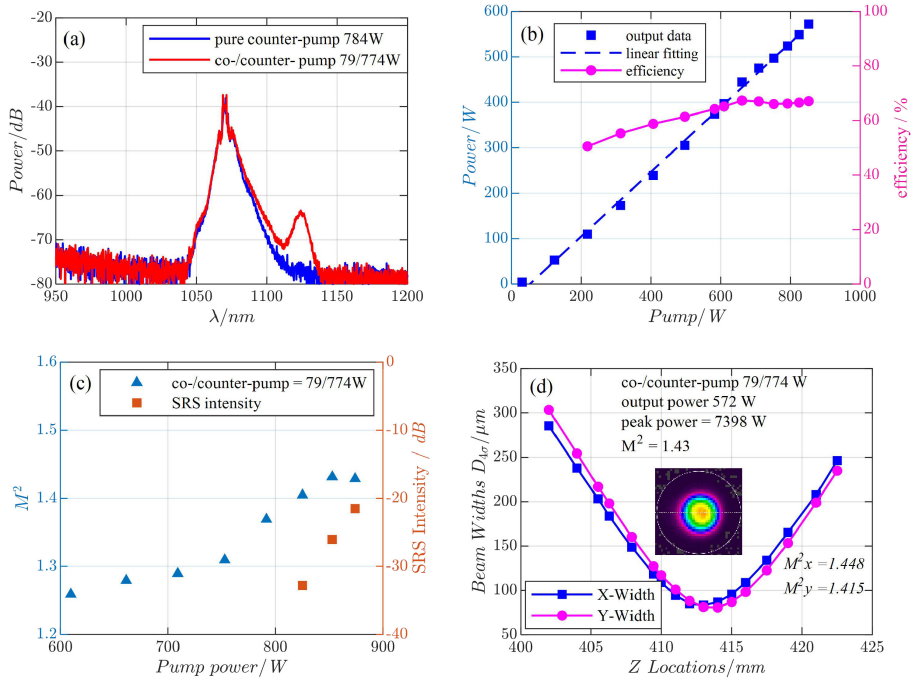

Fig. 5. Experiment results: (a) output spectrum; (b) variation curves of the output laser power and the efficiency; (c) beam quality and SRS intensity at different pump powers; (d) beam quality and profile at the maximum output power.

TABLE II
EXPERIMENTAL RESULTS WITH DIFFERENT OC-FBGS

No.	λ / nm	FWHM/nm	Reflectivity	P_{AVG} / W /	P_{peak} / W	M^2	P_{SRS} / dB
1	1069.94	1.01	9.5%	520	6414	1.28	-14.6
2	1069.95	1.01	5.5%	545	6515	1.32	-14.9
3	1069.89	2.0	9.5%	510	6035	1.31	-15.0

37.5/600 μm, to 25/400 μm. Its actual equivalent core diameter was 32.6 μm calculated under an equal volume assumption [16], and the absorption coefficient was about 1.5 dB/m at 976 nm. All the gain fiber was coiled in a racetrack groove with a diameter of 11.5-17.5 cm on the water-cooled plate. The FBGs had the same core/cladding diameter of 25/400 μm and the same center wavelength of 1070 nm. The reflectivity and full width at half maximum (FWHM) of high reflection fiber Bragg grating (HR-FBG) were 99.9%/4.09 nm. Three different OC-FBGs were separately used in the comparative experiments, whose OC-FBG reflectivity and FWHM were 9.5%/1.01 nm, 9.5%/2.0 nm, and 5.5%/1.01 nm, respectively. The FWHM of output laser approximated that of OC-FBG, which was much broader than the spectral width of the stimulated Brillouin scattering (SBS), hence the SBS gain could be negligible [17]. A section of GDF with a length of about 1 m was employed after the YDF to reduce the uncertainty caused by the fusion of gain fiber and different gratings, and the consequent impacts on the output power and nonlinear strength could be ignored [13]. Two (18+1)×1 pump&signal combiners were employed in the bidirectional-pumping configuration and all the LDs were loaded with the same driving current with a frequency of 1 kHz and duty cycle of 10% in the experiment. After the combiner, the laser light passed through a cladding power stripper (CPS) and emitted from a homemade coated quartz block head (QBH). The total length of the passive fiber after the combiner was about 3.5 m with a core/cladding diameter of 25/250 μm. A ∼9° angle was cleaved at the backward output port to reduce the feedback coefficient [18].

IV. RESULTS AND DISCUSSION

A. Results of Different OC Parameters

In order to verify the actual performance of the picked OC-FBG, a set of comparative experiments were conducted before the high peak power experiment. The main comparative results at the co-/counter-pump power of 74/679 W under 1 kHz repetition frequency and 100 μs pulse duration are shown in Table II. It can be seen that a lower reflectivity of OC-FBG is indeed beneficial for improving the output power, which is consistent with the simulation results, but the effect of increasing bandwidth of OC-FBG on SRS suppression is still insignificant, on factors of the inherently tiny difference caused by the slight bandwidth differences and the sampling error of spectrometer caused by the mismatch between the laser repetition and scanning speed of spectrometer.

B. Results of Optimized Parameters

Firstly, only the counter-pump was loaded into the system to get a good SRS suppression. When the maximum counter-pump power was achieved, the average output power was 535 W, with a

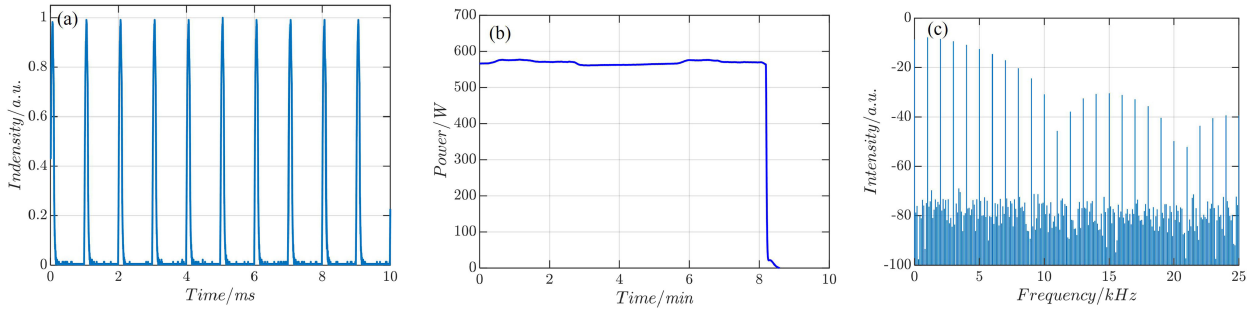

Fig. 6. The time-domain pulse profile at peak power of 7398 W (a), corresponding average output power fluctuation (b), and its FFT (c).

corresponding peak power of 7030 W and the SRS intensity was 35 dB lower than that of the signal light at the maximum power, as shown in Fig. 5(a)**.** The further power increase was limited by the available pump power. To increase the output power, a bidirectional-pumping scheme should be adopted.

Then, the co-/counter-pump power were simultaneously injected into the cavity in a proportion of about 1: 9.2, which was the minimum co-pump power ratio we could achieve by the limitation of the homemade circuit modulator. When the co-/counter-pump power increased to 79/774 W, the intensity of SRS increased to 26 dB lower than the signal, as shown in Fig. 5(a). The data points (blue square) and fitting curve in Fig. 5(b) show that there is a good linear relationship between the output and pump power. The optical efficiency is about 67% when the total pump exceeds 660 W. The small fluctuation of efficiency around 67% comes from the stability of the pump and measurement error, and the relatively low values at low pump power levels are due to the wavelength drift of the pump diodes. The output stability and measurement errors will be discussed in Section III.A. Further power scaling was limited by the rapidly increased SRS, as shown in Fig. 5(c)**,** so we didn't increase the co-/counter-pump power. The M^2 factor under 79/774 W pump power was 1.43, as shown in Fig. 5(d), where the value was calculated by the horizontal and vertical beam quality factors using $M^2 = \sqrt{M_x^2 \cdot M_y^2}$ [19], corresponding to an output peak power of 7398 W.

C. Analysis and Discussion

1) Output Stability: The oscillator had been continuously running for at least 8 minutes at the maximal co-/counter-pump power of 79/774 W under 1 kHz repetition frequency and 100 μs pulse duration, and the average value (AVG) and standard deviation (SD) of the peak and average output power were analyzed. The normalized time-domain pulse profile of a 10 μs long pulse train under the co-/counter-pump power of 79/774 W is shown in Fig. 6(a). It can be seen that the pulse sequence well maintains the repetition of 1kHz with the same stable peak power, corresponding to a normalized SD of 0.004 W. Larger scale average power fluctuations were recorded by the power meter under a sampling interval of 64 ms, as shown in Fig. 6(b). The average output power fluctuates within the range of 560.9 W to 577.0 W, where the average value is 568.9 W, and the standard deviation is 4.99 W. The actual fluctuation may be smaller, as the power meter fluctuates around zero by several watts within tens of seconds when there is no signal input. Even if calculated with the average value of 568.9 W, the peak power was 7359 W, corresponding to an exciting relative brightness of 31.4. To the best of our knowledge, this is the highest power and highest relative brightness of near-single-mode QCW fiber lasers.

2) Dynamic Characteristics: The sample interval of the oscilloscope was set at 0.1 μs, much smaller than the characteristic scale of SBS and TMI, and there were no typical dynamic characteristics of SBS or TMI found in the presented experiment. The FFT of the wave train presented in Fig. 6(a) is demonstrated in Fig. 6(c), and none of the other frequency components can be found except the eigenfrequencies of 1 kHz, 2 kHz, etc. Moreover, no phenomena such as power decline [20], rapid deterioration of beam quality [10], or waveform unstable [21] were found during the experiment. All of this indicated that the TMI had not occurred.

As mentioned before, the SBS is not the main consideration due to the broadband of output laser. In order to illustrate this point more intuitively, the spectrum and average power at the rear port of cavity were recorded, as shown in Fig. 7**.** It can be seen that, the spectrum is very smooth around 1070 nm without individual spikes, as shown in Fig. 7(a). Note that the high noise level of the spectrum is not characteristic for the laser but is due to mismatch between the laser repetition and scanning speed of spectrometer. The average power is significantly low (<0.5% of the average output power) and increases linearly, as shown in in Fig. 7(b), also indicating that there is no significant signal energy transfer to the Stokes of SBS.

V. Conclusion

In this manuscript, we have analyzed the current commercial products of QCW fiber laser and point out one key factor that affects the further scaling of output power, that is, the stiff balance between beam quality and SRS suppression. It is proposed that spindle-shaped gain fiber can be used to further improve the power and maintain a good beam quality. The appropriate gain fiber length and grating parameters can be determined by traditional rate equations, when considering the actual distribution of the pump spectrum. Finally, an optimized QCW fiber laser oscillator with a peak power of 7.3 kW was realized under the condition of a repetition frequency of 1 kHz and pulse width of 100 μs, with a corresponding pulse energy of 0.57 J and beam

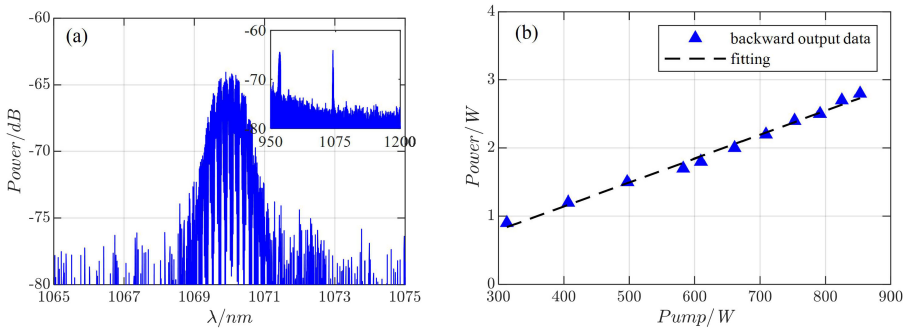

Fig. 7. The spectrum (a) and average power (b) at the rear port of the cavity.

quality M^2 factor ∼1.43, and an exciting relative brightness of 31.2. The stability is analyzed, and no TMI or SBS was observed in the experiment. It is the best performance of peak power and brightness in near-single-mode QCW fiber lasers at present, to the best of our knowledge.

ACKNOWLEDGMENT

The authors would like to thank Professor Jinyan Li's group of Huazhong University of Science and Technology for providing the excellent spindle-shaped YDF, and also thank Xiaoyong Xu, Zhejian Hong, Yun Ye, Lingfa Zeng, Pengfei Zhong and Penglin Zhong for technical supporting during the experiments.

REFERENCES

[1] D. J. Richardson, J. Nilsson, and W. A. Clarkson, "High power fiber lasers: Current status and future perspectives," *J. Opt. Soc. Amer. B*, vol. 27, no. 11, pp. B63–B92, 2010, doi: 10.1364/JOSAB.27.000B63.

[2] M. N. Zervas and C. A. Codemard, "High power fiber lasers: A review," *IEEE J. Sel. Topics Quantum Electron.*, vol. 20, no. 5, pp. 219–241, Sep./Oct. 2014.

[3] G. Luo, H. Xiao, S. Li, C. Wang, Q. Zhu, and L. Song, "Quasi-continuous-wave laser surface melting of aluminium alloy: Precipitate morphology, solute segregation and corrosion resistance," *Corrosion Sci.*, vol. 152, pp. 109–119, 2019, doi: 10.1016/j.corsci.2019.01.035.

[4] X. Hui, S. Li, H. Xu, J. Mazumder, and L. Song, "Laves phase control of Inconel 718 alloy using quasi-continuous-wave laser additive manufacturing," *Mater. Des.*, vol. 122, pp. 330–339, 2017.

[5] C. Leone, E. Mingione, and S. Genna, "Laser cutting of CFRP by quasi-continuous wave (QCW) fibre laser: Effect of process parameters and analysis of the HAZ index," *Composites Part B: Eng.*, vol. 224, 2021, Art. no. 109146, doi: 10.1016/j.compositesb.2021.109146.

[6] Z. Zhang, J. Zhang, Y. Wang, S. Zhao, X. Lin, and X. Li, "Removal of paint layer by layer using a 20 kHz 140 ns quasi-continuous wave laser," *Optik*, vol. 174, pp. 46–55, 2018, doi: 10.1016/j.ijleo.2018.08.057.

[7] H. Xiao, M. Cheng, and L. Song, "Direct fabrication of single-crystal-like structure using quasi-continuous-wave laser additive manufacturing," *J. Mater. Sci. Technol.*, vol. 60, pp. 216–221, 2021, doi: 10.1016/j.jmst.2020.04.043.

[8] Z. Hong, Y. Wan, X. Xi, H. Zhang, X. Wang, and X. Xu, "High-peak-power pump-modulated quasi-CW fiber laser," *Appl. Opt.*, vol. 61, no. 7, pp. 1826–1833, 2022, doi: 10.1364/AO.452604.

[9] L. Zeng *et al.*, "Near-single-mode 3 kW monolithic fiber oscillator based on a longitudinally spindle-shaped Yb-doped fiber," *Opt. Lett.*, vol. 45, no. 20, pp. 5792–5795, 2020, doi: 10.1364/OL.404893.

[10] L. Zeng *et al.*, "5 kW monolithic fiber amplifier employing home-made spindle-shaped ytterbium-doped fiber," *Opt. Lett.*, vol. 46, no. 6, pp. 1393–1396, 2021, doi: 10.1364/OL.418194.

[11] C. Shi, X. Wang, P. Zhou, X. Xu, and Q. Lu, "Theoretical study of mode evolution in active long tapered multimode fiber," *Opt. Exp.*, vol. 24, no. 17, pp. 19473–19490, 2016, doi: 10.1364/OE.24.019473.

[12] Y. Baolai *et al.*, "3.05 kW monolithic fiber laser oscillator with simultaneous optimizations of stimulated Raman scattering and transverse mode instability," *J. Opt.*, vol. 20, no. 2, 2018, Art. no. 025802.

[13] W. Liu, P. Ma, and P. Zhou, "Unified model for spectral and temporal properties of quasi-CW fiber lasers," *J. Opt. Soc. Amer. B*, vol. 38, no. 12, pp. 3663–3682, 2021, doi: 10.1364/JOSAB.439829.

[14] D. Hollenbeck and C. D. Cantrell, "Parallelizable, bidirectional method for simulating optical-signal propagation," *J. Lightw. Technol.*, vol. 27, no. 12, pp. 2140–2149, Jun. 2009, doi: 10.1109/JLT.2008.2009471.

[15] T. Schreiber *et al.*, "Analysis of stimulated Raman scattering in cw kW fiber oscillators," in *Proc. Int. Soc. Opt. Eng.*, 2014, vol. 8961, Art. no. 89611T, doi: 10.1117/12.2039869.

[16] Y. Ye *et al.*, "Comparative study on transverse mode instability of fiber amplifiers based on long tapered fiber and conventional uniform fiber," *Laser Phys. Lett.*, vol. 16, no. 8, 2019, Art. no. 085109, doi: 10.1088/1612-202x/ab2acf.

[17] G. P. Agrawal, *Nonlinear Fiber Optics*, 6th ed. San Diego, CA, USA: Academic, 2019.

[18] Y. Ye *et al.*, "Experimental study of 5-kW high-stability monolithic fiber laser oscillator with or without external feedback," *IEEE Photon. J*, vol. 11, no. 4, Aug. 2019, Art. no. 1503508, doi: 10.1109/JPHOT.2019.2923709.

[19] "Lasers and laser-related equipment - Test Methods for laser beam widths, divergence angles and beam propagation ratios – Part 2: General astigmatic beams," ISO 11146-2-2005, 2005.

[20] V. Scarnera, F. Ghiringhelli, A. Malinowski, C. A. Codemard, M. K. Durkin, and M. N. Zervas, "Modal instabilities in high power fiber laser oscillators," *Opt. Exp.*, vol. 27, no. 4, pp. 4386–4403, 2019, doi: 10.1364/OE.27.004386.

[21] N. Haarlammert *et al.*, "Build up and decay of mode instability in a high power fiber amplifier," *Opt. Exp.*, vol. 20, no. 12, pp. 13274–13283, 2012, doi: 10.1364/OE.20.013274.